MNRAS 543, 2058-2077 (2025) Advance Access publication 2025 August 13

V Sge: supersoft source or exotic hot binary? – I. An X-Shooter campaign in the high state

Pasi Hakala . 1 Phil Charles 2,3,4 and Pablo Rodríguez-Gil . 5,6

- ¹Finnish Centre for Astronomy with ESO (FINCA), Quantum, FI-20014, University of Turku, Finland
- ²Department of Physics & Astronomy, University of Southampton, Southampton SO17 1BJ, UK
- ³Astrophysics, Department of Physics, University of Oxford, Keble Road, Oxford OX1 3RH, UK
- ⁴Department of Physics, University of the Free State, PO Box 339, Bloemfontein 9300, South Africa
- ⁵Instituto de Astrofísica de Canarias, E-38205 La Laguna, Tenerife, Spain

Accepted 2025 July 30. Received 2025 July 30; in original form 2025 March 6

ABSTRACT

V Sge is a peculiar, highly luminous long-period (12.34 h) binary star that can display a supersoft X-ray emitting component when in the faint phase of its $V \approx 10-13$ mag variability range. Apparently undergoing Eddington-limited accretion from its more massive secondary, it is in a very rare, short-lived evolutionary phase towards the double degenerate channel. Its complex and highly variable optical emission features, from Balmer and He II to high-ionization lines, including strong fluorescence features, have been challenging to interpret, especially given the absence of any absorption lines associated with photospheric features from either stellar component. With the detailed properties of V Sge, especially the donor, still controversial, we undertook a VLT/X-Shooter campaign over 4 months in 2023, obtaining high Signal-to-noise ratio, high resolution spectra that revealed multiple components in both high- and low-ionization lines. This allows us to track V Sge's principal emitting regions via Doppler tomography, obtaining new insights into high accretion-rate dynamics. In particular, we identify a stationary, double-peaked emission core which we interpret as a circumbinary ring, analogous to SS 433. This enables us to derive limits on the system masses. Furthermore, we find very broad emission-line wings whose mean velocity can vary over hundreds of kilometres per second on time-scales of decades, yet 'flip' between states in <1 week. We show that the supersoft X-ray source interpretation is able to account for these and other observational attributes significantly better than the hot binary model, concluding that V Sge could be one of the brightest known Galactic supersoft sources.

Key words: accretion, accretion discs – binaries (including multiple): close – (stars): circumstellar matter.

1 INTRODUCTION AND BACKGROUND TO **V SGE**

V Sge is a luminous ($L_{\text{bol}} = 10^{37} \text{ erg s}^{-1}$) Galactic variable binary system that has been known since 1902 and has an orbital period of $P_{\rm orb} = 12.34 \, \rm h$. Herbig et al. (1965), hereafter H65, identified its binary nature through both photometry and spectroscopy, concluding that it contained two evolved, hot stars of masses 0.7 and 2.8 M_{\odot} , the nature of which has remained controversial ever since. Extensive modelling of the eclipsing light curve, assuming a pure binary model without any disc (e.g. Smak, Belczynski & Zola 2001) indicated a binary inclination of 71°. The system exhibits high and low optical states (ranging over $V \approx 10.0 - 13.0 \,\mathrm{mag}$), which are possibly linked to changes in the accretion rate. A variety of models have been proposed and were most recently reviewed in Smak et al. (2001), including that of a nova-like variable, a supersoft X-ray source (SSS), and a hot contact binary. Furthermore, it now has a Gaia DR3-established distance of $3.02 \pm 0.19 \,\mathrm{kpc}$ (Gaia Collaboration 2023), making it a very luminous object. Indeed, even in its faint state, V Sge has a luminosity \sim 100 times greater than typical novalike variables (Abril et al. 2020).

It was noted by Šimon & Mattei (1999) that, in modelling the high state, the optical emission likely includes an additional, non-eclipsed component, as a consequence of the extremely high mass-loss rate from the donor, leading to the presence of circumbinary matter, as well as emission from an accretion disc wind (see also top panel of fig. 3 in Hachisu & Kato 2003). Occasionally, the high and low states seem to alternate with a cycle time of approximately 1 month (Kato 2004). Various alternative models have been proposed, including hot detached binaries with colliding winds (Lockley et al. 1999; Wood & Lockley 2000) or a hot binary submerged in a hot cocoon (Smak et al.

The optical spectrum of V Sge is complex. The emission lines are not clearly double-peaked, which would typically indicate an accretion disc, but they occasionally exhibit P Cygni profiles, resembling the SW Sex behaviour in cataclysmic variables (Thorstensen et al. 1991; Rodríguez-Gil et al. 2007). Strong emission lines of He II λ4686 and the Balmer series, along with additional very high excitation lines (e.g. O VI and N V), are present in the spectrum, sometimes showing sharp, multiple components that vary with orbital Downloaded from https://academic.oup.com/mnras/article/543/3/2058/8233646 by University of Southampton user on 17 November 2025

⁶Departamento de Astrofísica, Universidad de La Laguna, E-38206 La Laguna, Tenerife, Spain

^{*} E-mail: pahakala@utu.fi

phase (H65). Both He II and H β vary over the orbit, and Diaz (1999) attempted to Doppler map (Marsh & Horne 1988) the emission regions. However, this effort had limited success, likely due to the presence of significant vertical structure in the system. Such structure introduces velocity components perpendicular to the orbital plane, thereby violating a fundamental assumption of Doppler tomography. Consequently, the geometry underlying the complex and variable emission-line profiles remains poorly constrained.

Finally, the inferred high inverse mass ratio of the system, $q = M_2/M_1 \approx 3$, with M_1 and M_2 the masses of the accretor and the donor, primarily relies on the OIII fluorescent line radial velocity shifts observed by H65. These emission lines (O III λ3133 and $\lambda 3444$) are reported to consist of two components that oscillate in antiphase over the orbital period (see fig. 4 in H65). However, closer inspection of the radial velocity values in H65 reveals that the modulation is clearly not sinusoidal but instead shows constant radial velocities covering approximately one-third of the orbital cycle. Furthermore, abrupt transitions occur from large positive to large negative velocities at, or near, phase 0.0, casting doubt on whether the two O III components represent the intrinsic radial velocities of the binary components. In fact, we demonstrate here that the two components in the O III lines correspond to the narrow double-peaked core emission found in all emission lines, with the primary distinction being the lack of high velocity components in the O III features.

1.1 Evidence for the SSS component in V Sge

The earliest soft X-ray detections of V Sge were reported in Eracleous, Halpern & Patterson (1991), based on archival Einstein Observatory IPC images, and Hoard, Wallerstein & Willson (1996) (see their appendix), using *ROSAT* observations of PU Vul, which fortuitously had V Sge in the field of view (albeit 31 arcmin offaxis). These *ROSAT* data recorded an X-ray spectral hardness ratio indicative of 'very soft X-rays', but no spectral modelling was undertaken.

More importantly, Greiner & Teeseling (1998), Patterson et al. (1998), and Steiner & Diaz (1998) noted that V Sge had four key properties:

- (i) presence of O VI and N V emission;
- (ii) a ratio of He II/H β emission > 2;
- (iii) high V-band absolute magnitude, M_V ; and
- (iv) a deep, wide primary eclipse,

which were all very similar to the known SSS binaries, thereby providing strong circumstantial evidence for including V Sge among them. Classical SSSs are accretion-powered interacting binaries where a white dwarf (WD) primary accretes matter from, in most cases, a more massive, Roche lobe-filling companion (Kahabka 1997). Due to the inverted mass ratio, accretion in SSSs is a self-accelerating process, meaning that they represent a short-lived, but very violent phase in binary evolution. Consequently, the accretion rate in SSSs can be very high ($\sim 10^{-7}~\dot{\rm M}_\odot~\rm yr^{-1}$), thereby enabling sustained thermonuclear burning of the accreted matter on the surface of the WD, and allowing SSSs to reach Eddington-limited X-ray luminosities, typically a 1000 times greater than in normal cataclysmic variables.

The X-ray emission of SSSs is characterized by a very low temperature ($\sim 10^5$ K) and a very high luminosity ($L_{\rm X} > 10^{36}$ erg s⁻¹) for a WD compact object due to the high accretion rate (van den Heuvel et al. 1992). Few SSS candidates are known in the Galaxy because of their extremely soft X-ray spectrum and the high levels of extinction in the Galactic plane; accordingly, far more have

been identified in the Magellanic Clouds. The optical emission of SSSs is primarily driven by X-ray reprocessing in the accretion disc surrounding the WD. Meyer-Hofmeister, Schandl & Meyer (1997) modelled the optical light curves of SSSs, demonstrating that the accretion disc rim must be vertically extended, likely due to the impact of the high-rate accretion stream on the outer disc.

Furthermore, it had already been well established for the prototypical SSSs, CAL83 and RX J0513.9–6951, that the very soft X-ray component was visible only when the system was in a faint state (Southwell et al. 1996), a property already noted as analogous to that of the VY Scl CV-sub-class (Steiner & Diaz 1998). Since state changes are unpredictable, Greiner & Teeseling (1998) summarize all the *ROSAT* observations in their table 1, making it clear that only a single interval (May 1994) contained V Sge in a faint state and this yielded the highest X-ray count rate seen by *ROSAT*. Unfortunately, that was using the HRI (High Resolution Imager) detector, which nominally has no spectral capability. But Greiner & Teeseling exploited the onboard HRI PH-channel distributions of those data to show that they were completely different (contained in low energy channels only) compared to the bright state's harder X-ray data. We re-examine these data later.

Unfortunately, V Sge has remained almost permanently in the high state in recent times, preventing further faint-state observations with the currently available soft X-ray facilities (Swift, Einstein Probe, eRosita). When it next enters a faint state, new observations should be undertaken without delay.

1.2 A new campaign

In spite of many extensive and multiwavelength observing campaigns in the decades since H65, V Sge displays peculiarities that have defied explanation within standard interacting binary models. While the photometric light curves have been well established, it has proved much harder to obtain comparable high quality spectroscopic coverage across the full orbital cycle because of its awkward 12.34-h orbital period. Here, we bring a new approach to investigating the various emitting components in V Sge by exploiting the superb wavelength coverage (3000 Å $-2.5\,\mu$) and spectral resolution of X-Shooter spread over a \approx 4-month period so as to obtain the highest S/N optical/near-infrared (NIR) spectra of V Sge yet, and with uniform phase coverage, all in the high state.

2 OBSERVATIONS

V Sge was the target of our X-Shooter campaign between June and September 2023 (proposal 111.24YF). X-Shooter is a versatile, medium-resolution spectrograph located at the Very Large Telescope (VLT; Vernet et al. 2011). Designed to cover a broad wavelength range, from the ultraviolet (3000 Å) to the NIR (25000 Å) in a single exposure, it provides simultaneous spectral coverage in three bands: ultraviolet-blue (UVB), visual (VIS), and NIR. With its medium spectral resolution ($R \approx 4000-18000$), it is well suited for both radial velocity and line profile studies. Given the brightness of V Sge, it was observed as a filler target for less than ideal conditions, yielding approximately 60 good quality spectra over the 120-d observing period (60, 58, and 55 in the UVB, VIS, and NIR bands, respectively). Even though these spectra were taken at random times, they adequately sample the 12.34-h orbital period of. We used 1, 0.9, and 0.9 arcsec slits in the UVB, VIS, and NIR bands, respectively. This yielded spectral resolutions of approximately 5400, 8900, and 5600 in the same bands, respectively. No on-chip binning was applied.

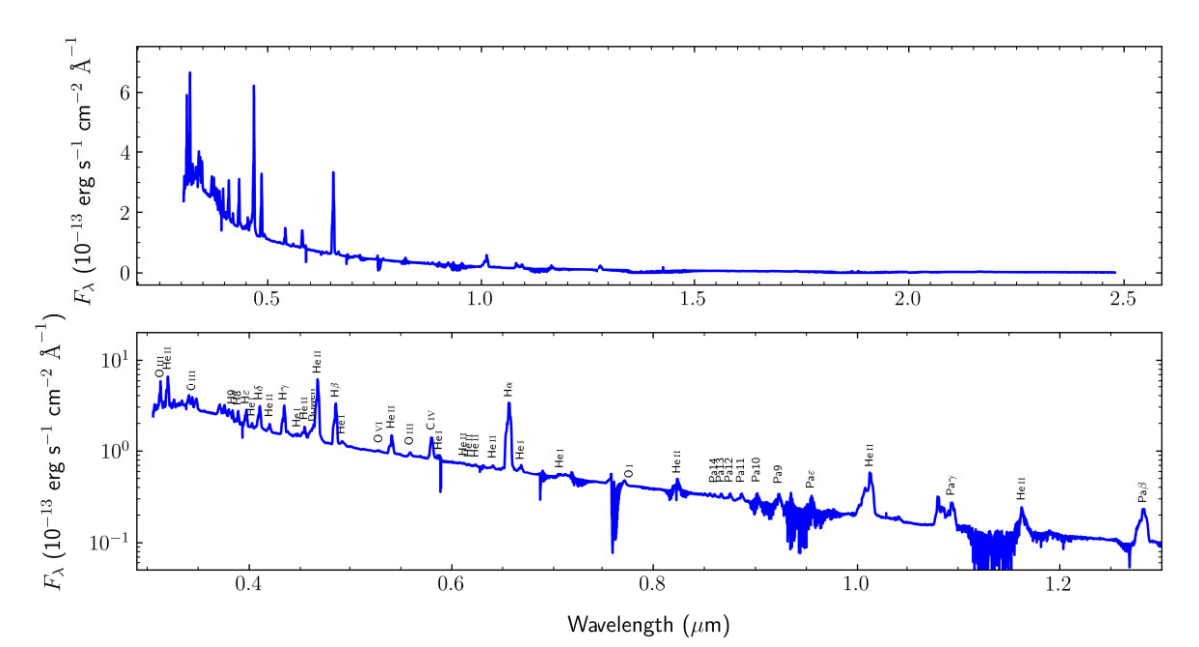


Figure 1. X-Shooter mean spectrum of V Sge in the high state on linear (upper) and logarithmic (lower) flux scales. The observed fluxes were corrected for interstellar reddening using E(B-V) = 0.11. An online interactive version of the top panel plot is available at https://tinyurl.com/3tptc798.

The X-Shooter spectra were reduced using the ESOREFLEX automated pipeline (Freudling et al. 2013) together with the X-Shooter workflow. This produces spectra corrected from the instrumental response; however, as our observations were conducted under non-optimal conditions, the flux calibrations are, in many cases, unreliable. Nevertheless, intensive monitoring of V Sge by AAVSO¹ showed that it remained in the high state throughout, with a mean magnitude of $V \approx 11$. The barycentric correction was also applied to the spectra (both in time and velocity).

3 THE X-SHOOTER SPECTRA

The overall spectrum of V Sge is shown in Fig. 1. The reader can use the online zoom function in order to inspect any part of the spectrum in detail. The emission is dominated by a very blue continuum, accompanied by a plethora of strong emission lines with complex profiles. The strongest lines include the hydrogen Balmer series, various He II lines, as well as O III and O IV lines (see Figs 2, 3, and Appendix A). Notably, there are no clear absorption lines that could be associated with either stellar component. Detailed trailed spectra diagrams of all significant emission lines, from UVB to NIR, are presented in Appendix A (Figs A1-A3).

All data were imported into MOLLY² to prepare them for trailed spectrograms and to measure the emission line radial velocity curves. For simplicity, the orbital phase was computed using the linear eclipse ephemeris from Zang et al. (2022), with P=0.5141923 d, and a zero-phase time of $T_0({\rm HJD})=2460096.825$, derived from minima in AAVSO white-light (CV) and V-band light curves. The orbital phase shifts relative to the cubic ephemeris of Smak (2022) and the quadratic ephemeris of Zang et al. (2022) are approximately 0.014 and 0.011 cycle, respectively, which we consider negligible.

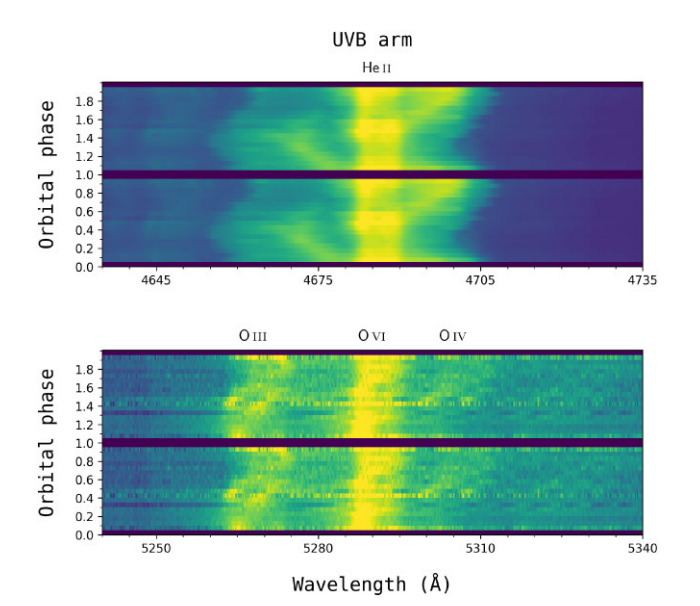


Figure 2. Trailed spectrograms showing the $\text{He II}\,\lambda4686$ (upper) and $O\,\text{VI}\,\lambda5290$ (lower) emission lines. The spectra have been phase-binned into 20 orbital phase intervals and repeated once for display purposes. The dark horizontal stripes are bins containing no data. Note the systematic *blueshift* of the He II broad line component.

3.1 Emission line profiles

3.1.1 Stationary double-peaked core (the 'tram lines')

The strongest emission lines in V Sge share a variety of common features showing similar variability (and non-variability) over the orbital period. Perhaps the most striking feature of almost all emission line profiles is the prominent, double-peaked narrow core emission with peaks at radial velocities of ± 150 –200 km s⁻¹ (Fig. 2, top). This narrow line core is centred at the rest velocity and does

¹The American Association of Variable Star Observers: aavso.org.

²https://cygnus.astro.warwick.ac.uk/phsaap/software/molly/html/INDEX.html

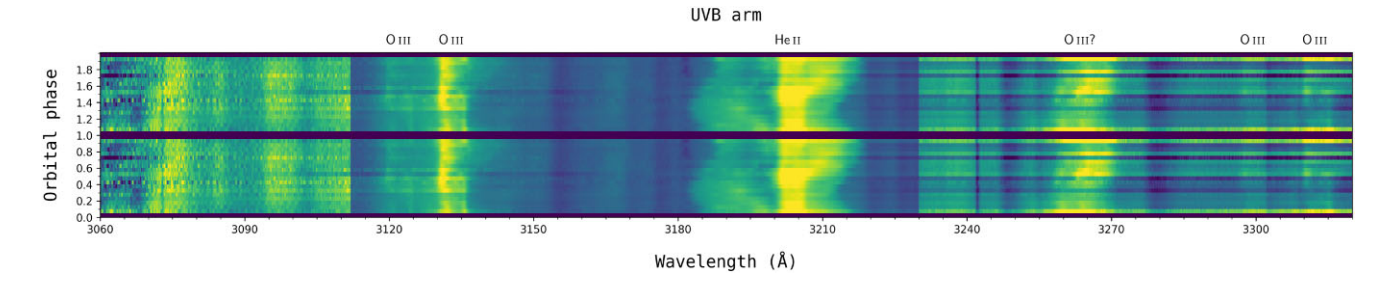


Figure 3. Trailed spectrogram showing the region around He II λ 3203. The spectra are phase-binned as described in Fig. 2. Different contrast levels have been used in order to enhance the fainter lines, and one orbital cycle has been repeated for display purposes.

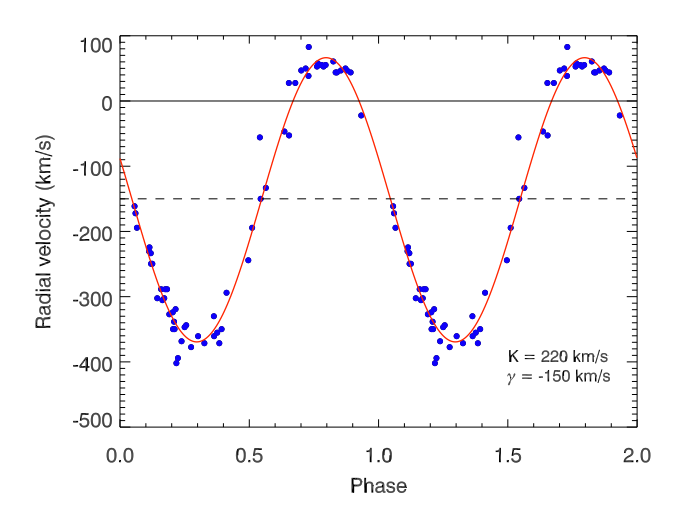


Figure 4. Radial velocity curves of the He II λ 5411 emission lines (blue dots) derived from the double-Gaussian and wing-folding methods (Appendix B). The best-fitting sinusoid is shown in red. The radial velocity values for the individual spectra are plotted twice for clarity.

not show any movement over the orbital period. This component, which has previously appeared as mostly flat-topped (due to spectral resolution limitations), is clearly double peaked in *all* lines. Notably, the velocities of the two peaks are close to those reported in H65 as the orbital velocity of the less massive component in the system.

3.1.2 Doppler-shifted very broad component

Intriguingly, the Balmer and He II lines also show a very broad emission component with a full width at zero intensity of FWZI = 3250 km s⁻¹, which appears to follow the motion of the presumed WD (which is eclipsed at phase 0.0). We have studied the dynamics of the broad emission component as a function of orbital phase employing the double-Gaussian method commonly used for modelling the wing motion of strong broad emission lines (Schneider & Young 1980; Shafter 1983). We have also developed another similar approach, and chosen He II $\lambda 5411$ to carry out the analysis, as the He II λ4686 blue wing is contaminated by the Bowen blend. The details of our new 'wing-folding' method, and the double diagnostic diagrams are shown in Appendix B. As a result, we find that the overall velocity shift of the broad component is $-150 \,\mathrm{km \ s^{-1}}$ relative to the V Sge systemic velocity and the double-peaked core component. Our analysis also reveals that the broad component exhibits a velocity modulation which follows the motion of the primary (see Fig. 4), and implies $K_1 = 200-250 \,\mathrm{km \ s^{-1}}$ for $i = 90^\circ$

and $K_1 = 220-275 \,\mathrm{km \ s^{-1}}$ for $i = 65^\circ$, which we presume as the lower limit for the inclination, given the partly eclipsing nature of the system. This strongly suggests that the broad component may carry a wind velocity component towards the observer in addition to the orbital motion. This will be discussed in detail later.

The same emission lines also show evidence of a third, higher velocity component that appears as an increasingly blue-shifted protrusion at phases 0.0–0.5 and as a red-shifted protrusion at phases 0.5–1.0. This component reaches radial velocities of at least up to $\pm 1000 \, \mathrm{km \ s^{-1}}$, and its velocity phasing is consistent with that of a possible accretion flow *around* the WD. This is likely related to V Sge being Eddington-limited in the high state and this is producing an irradiation-driven outflow (or wind) from the inner disc, and possibly the WD surface. In fact, at $M_V = -3.73 \, \mathrm{mag}$ in the highest state, V Sge is intrinsically the most luminous of the known SSSs (Šimon 2003).

3.1.3 Blue-shifted absorption component

The He I emission lines (at 3867, 4026, 4471, 5016, and 5876 Å) exhibit a fundamentally different profile from the Balmer and He II lines. Each features a strong, phase-dependent, and blueshifted absorption component with intriguing behaviour. The He I trailed spectra suggest a blue-shifted absorption component that steadily increases in velocity throughout the orbital cycle, reaching its maximum blue shift just before the phase gap covering the eclipse. However, a detailed inspection of He I \(\lambda 4471\) (Fig. 5) in each individual spectrum reveals a strong, narrow absorption feature at -500 or $-600 \,\mathrm{km} \,\mathrm{s}^{-1}$, which is pre-dominantly present around phase 0.0. At other phases, the absorption varies more in both width and central velocity. Moreover, its strength is significantly weaker at those phases. The combination of these effects results in the apparent phase-dependent blue-shifted behaviour observed in the He I trailed spectra. We have marked the spectra exhibiting strong blue-shifted absorption with their corresponding orbital phase in Fig. 5. We note that this feature was previously observed by H65 and by Iijima, Naito & Narusawa (2024). The phasing of this blue-shifted absorption is particularly intriguing, as it suggests that cooler matter might be escaping the system from behind the donor star, i.e. through the binary's L2 point. We will explore this further in Section 5.

3.2 Doppler tomograms

We have reservations about the application of Doppler tomography to a system such as V Sge, where significant vertical structures are likely present, leading to possible vertical velocity components and orbital-phase-dependent visibility issues with parts of the accretion disc, assuming geometries such as that proposed by Hachisu & Kato

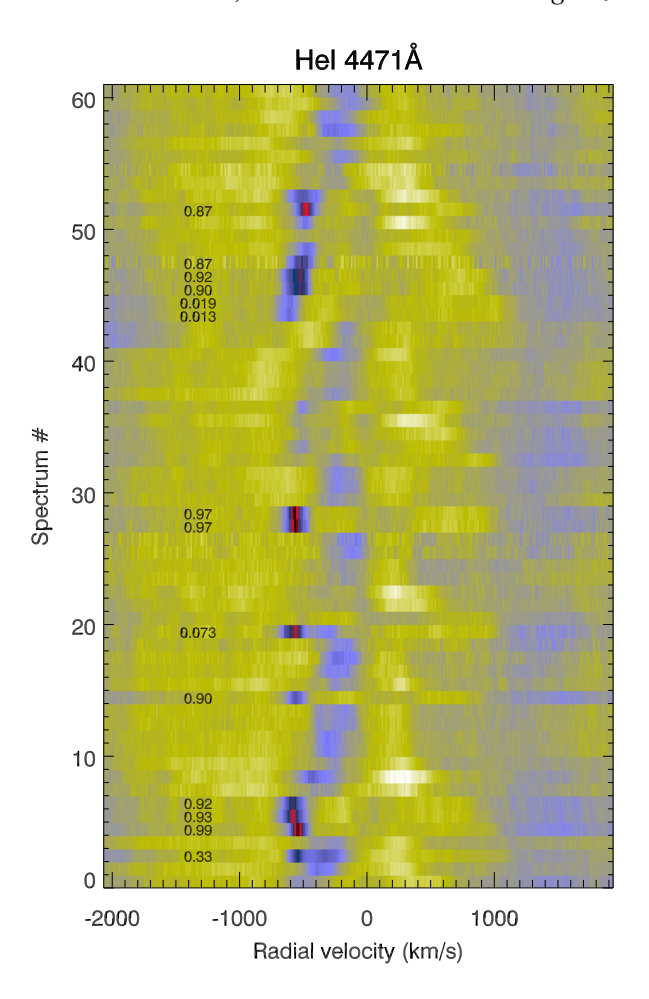


Figure 5. The individual spectra around He1 λ 4471 in velocity space, ordered by spectrum number. The 61 spectra span an interval of \approx 4 months, with time running from bottom to top. Spectra exhibiting strong blue-shifted He1 absorption have been marked with their respective orbital phase.

(2003). Nevertheless, we have conducted Doppler tomography of selected strong emission lines, as their principal orbital behaviour appears stable over extended intervals.

For this, we used the DOPMAP package of Spruit (1998), which employs a maximum entropy approach for Doppler mapping, enabling comparison of model trailed spectrograms with those derived from the data. DOPMAP proceeds by first fitting and subtracting the continuum around the chosen line before producing the maximum entropy solution for the Doppler map. We selected all Balmer lines, as well as He II and O III, and the resulting tomograms are shown in Fig. 6. We used $\gamma=0.0~{\rm km\,s^{-1}}$ for our Doppler analysis. The dominant feature in almost all Doppler maps is a bright central ring around the velocity origin. This ring has a typical radius of 150–180 km s⁻¹ and manifests as the line core 'tram lines' in all the trailed spectrograms. There is no indication of any radial velocity changes associated with the 'tram lines' structure itself.

Additionally, extra emission appears in the south–east quadrants of the maps (i.e. positive V_x , negative V_y), which could be linked to matter that has undergone a slingshot around the WD – possibly a quasi-ballistic accretion stream above the disc due to Eddington-limited accretion occurring in the high state, as mentioned earlier. Notably, the fluorescent O III lines (at 3133 and 3444 Å) also exhibit the same central emission ring but are much weaker at higher velocities.

Finally, the C IV line at 5804 Å shows markedly different behaviour compared to all other lines. It is the only one that does *not* display clear, non-variable 'tram lines' in its core. Moreover, its overall profile appears to follow the motion of the WD more clearly than any other line.

4 ARCHIVAL SOFT X-RAY OBSERVATIONS

As summarized in Section 1, there has only been one X-ray observation of V Sge in the faint state (Greiner & Teeseling 1998), when the soft X-rays of a SSS component are typically visible. However, in a study of four VY Scl nova-like systems, Zemko et al. (2014) noted that they could detect no SSS component during any of their high or low state observations. They go on to state that V Sge 'had not been actually observed as SSS', which contradicts the work of Greiner & Teeseling (1998). Accordingly, we have independently re-extracted the *ROSAT* source events for the two HRI observations in the bright and faint states, and in Fig. 7 show the faint state (red) and bright state (blue) PH distributions. To investigate the formal significance of this result, we performed a Kolmogorov–Smirnov test which gave a probability of 1.1×10^{-6} that these two samples come from the same distribution. This clearly demonstrates the presence of an SSS component at that time.

5 DISCUSSION

Our VLT/X-Shooter data provide an unprecedented spectral overview of V Sge, given the wide wavelength coverage and resolution. Despite – and perhaps because of – the quality and high S/N of these spectra, they are raising important questions regarding the nature of V Sge.

5.1 Do we know the basic binary parameters?

Our current understanding of V Sge remains largely based on the initial spectroscopic study by H65, which continues to serve as the foundation for nearly all subsequent investigations. The key properties identified by H65 are:

- (i) two spectral line components varying in antiphase, implying a mass ratio of q=3.8; and
 - (ii) component masses of $M_1 = 0.74 \,\mathrm{M}_\odot$ and $M_2 = 2.8 \,\mathrm{M}_\odot$.

Our primary concern regarding these properties is that, unlike most spectroscopic binary studies, V Sge is a purely *emission-line* object, with these estimates mainly derived from O III $\lambda 3444$ and O VI $\lambda 3811$ measurements. We examined the O III $\lambda 3133$ and $\lambda 3444$ lines in our data set but found no clear evidence of two components moving in antiphase (Fig. 8). Moreover, as already mentioned in Section 1, upon closer inspection, the original radial velocity curves of H65 do *not* exhibit a sinusoidal variation but instead show two components moving at constant velocities, with their relative strengths varying over $P_{\rm orb}$ – much as is seen in our data. This raises the crucial question of whether we truly know the masses of the two stars in V Sge. We believe that the masses (and mass ratio) could well be quite different from what has been assumed in the past, as will be demonstrated next.

5.2 Is there a circumbinary ring in V Sge?

Our spectra cover the full X-Shooter range from 3000 to 24 000 Å, and the plethora of detected emission lines includes the Balmer, Paschen, and Brackett series, numerous He I and He II lines, as

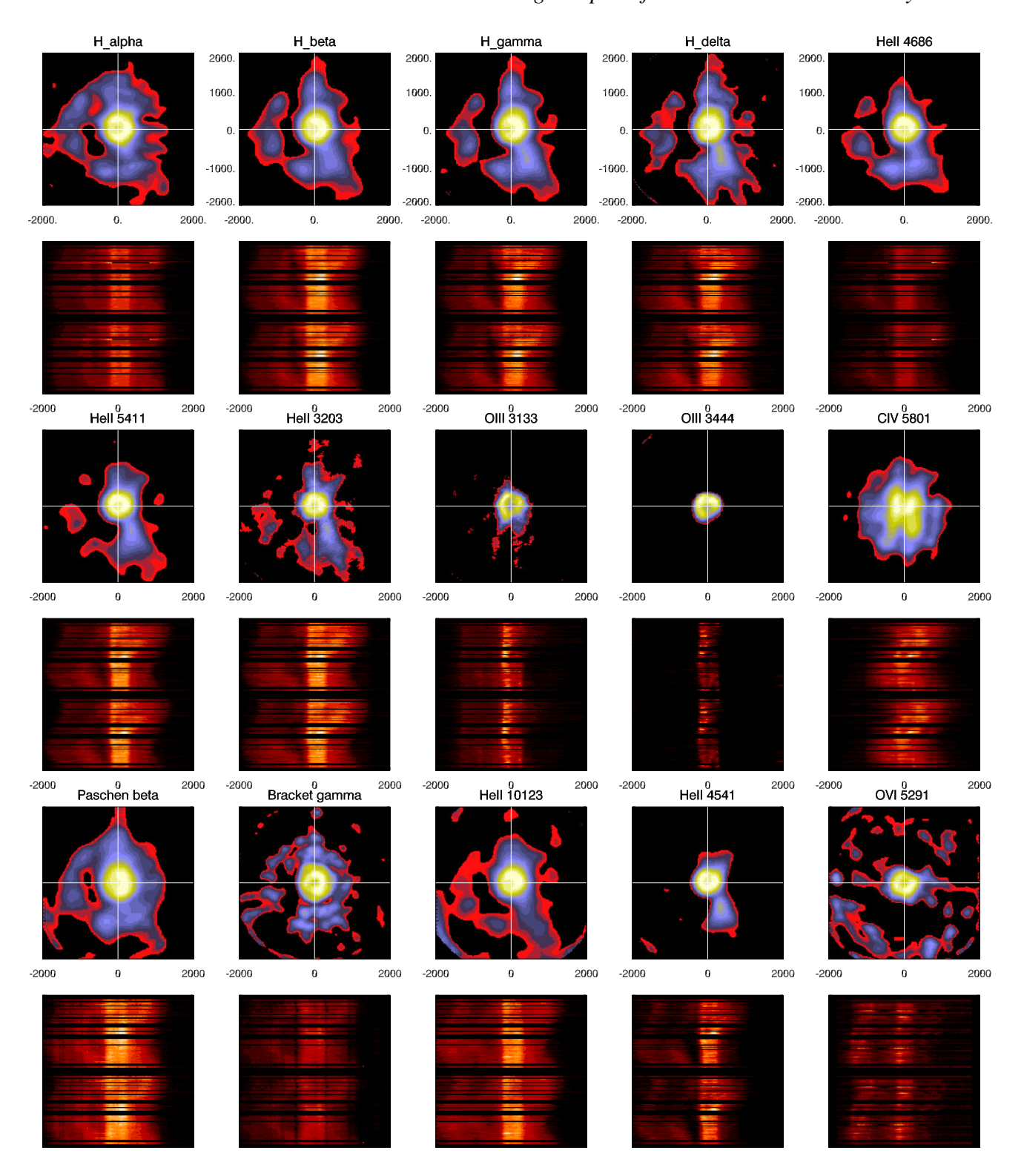


Figure 6. Selected Doppler tomograms of various emission lines. For each line, we present the Doppler tomogram (top) and the corresponding trailed spectrogram (bottom). In the tomograms, the axes represent velocity coordinates V_x and V_y in km s⁻¹. In the trailed spectrograms, the x-axis indicates velocity in km s⁻¹, and the y-axis shows the orbital phase. For clarity, the trailed spectra are repeated over two orbital cycles.

well as higher ionization lines such as OIII, OIV, and CIV. A key feature revealed by our high spectral resolution is that most of these lines typically exhibit a narrow, double-peaked emission feature (the 'tram lines' mentioned in Section 3.2), with a peak

separation of ± 150 – $180 \, \mathrm{km \ s^{-1}}$. More importantly, (a) this feature does *not* vary with orbital phase, and (b) is centred at the systemic velocity, meaning that *these emission features do not follow the motion of either stellar component*. We have measured the orbital

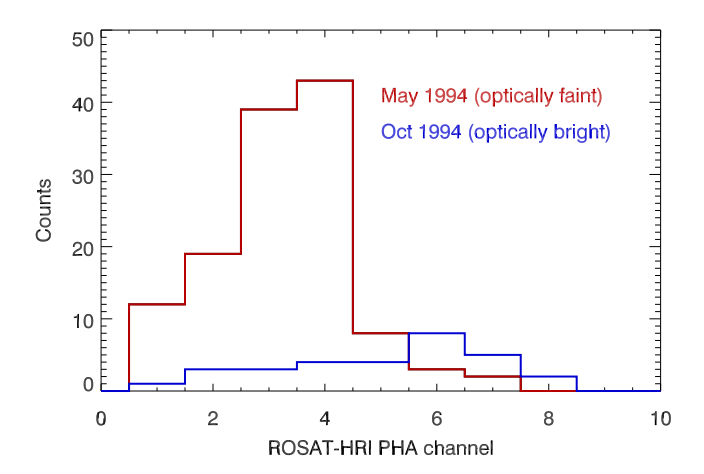


Figure 7. Soft X-ray pulse-height spectra of the *ROSAT* observations of V Sge with the HRI detector in the faint state of May 1994 (red) and the bright state of October 1994 (blue). PHA channel is proportional to X-ray energy, covering a range of $\approx 0.1 - 2.4 \, \text{keV}$.

velocity of the circumbinary ring using two different methods. First, we measure the radius of the central ring in the Doppler maps in eight different strong lines (Table 1) in both X- and Y-directions. This resulted in circumbinary ring velocities $\sim 155 \, \mathrm{km \ s^{-1}}$. Secondly, we have fitted the mean H α profile with a model consisting of seven Gaussian profiles (Fig. 9) applying the differential evolution (DE) global optimization algorithm (Storn & Price 1997). We then bootstrapped the errors from this fit. This produced a circumbinary ring velocity of $159 \pm 5 \, \mathrm{km \ s^{-1}}$, compatible with the first method.

Table 1. Estimated circumbinary ring orbital velocities a for different Doppler map emission lines.

Line	$V_{\text{circ},x}$ (km s ⁻¹)	$V_{\text{circ},y}$ (km s ⁻¹)
Нα	181	193
Нβ	154	166
Нγ	154	166
Нδ	143	158
Не п λ3203	132	132
Не п λ4686	159	154
Не п λ5411	153	145
Не п λ10123	147	152
$ar{V}_{ m circ}$:	158 ± 7	153 ± 5

Note. ^a The two columns relate to measuring the velocity profile of the central map in the *x*- and *y*-directions.

This analysis also produced an estimate for the systemic velocity, i.e. $\gamma=28.6\pm1.9~\rm km~s^{-1}$. We believe the only plausible explanation for this behaviour is that they originate from a circumbinary ring or disc of matter that has escaped the binary.

We have simulated the formation of such a ring using the binary magnetic accretion code HYDISC (King 1993; Wynn & King 1995). To expel matter from the system, we introduced a 'magnetic propeller' WD as the compact object, providing an additional 'kick' to the matter when it falls on a ballistic trajectory past the WD. We then adjusted this 'kick' to be as small as possible while still enabling at least some matter to escape the WD's Roche lobe. It is important to emphasize that we are not suggesting that V Sge contains a magnetic, spinning WD; rather, we use this simply as a

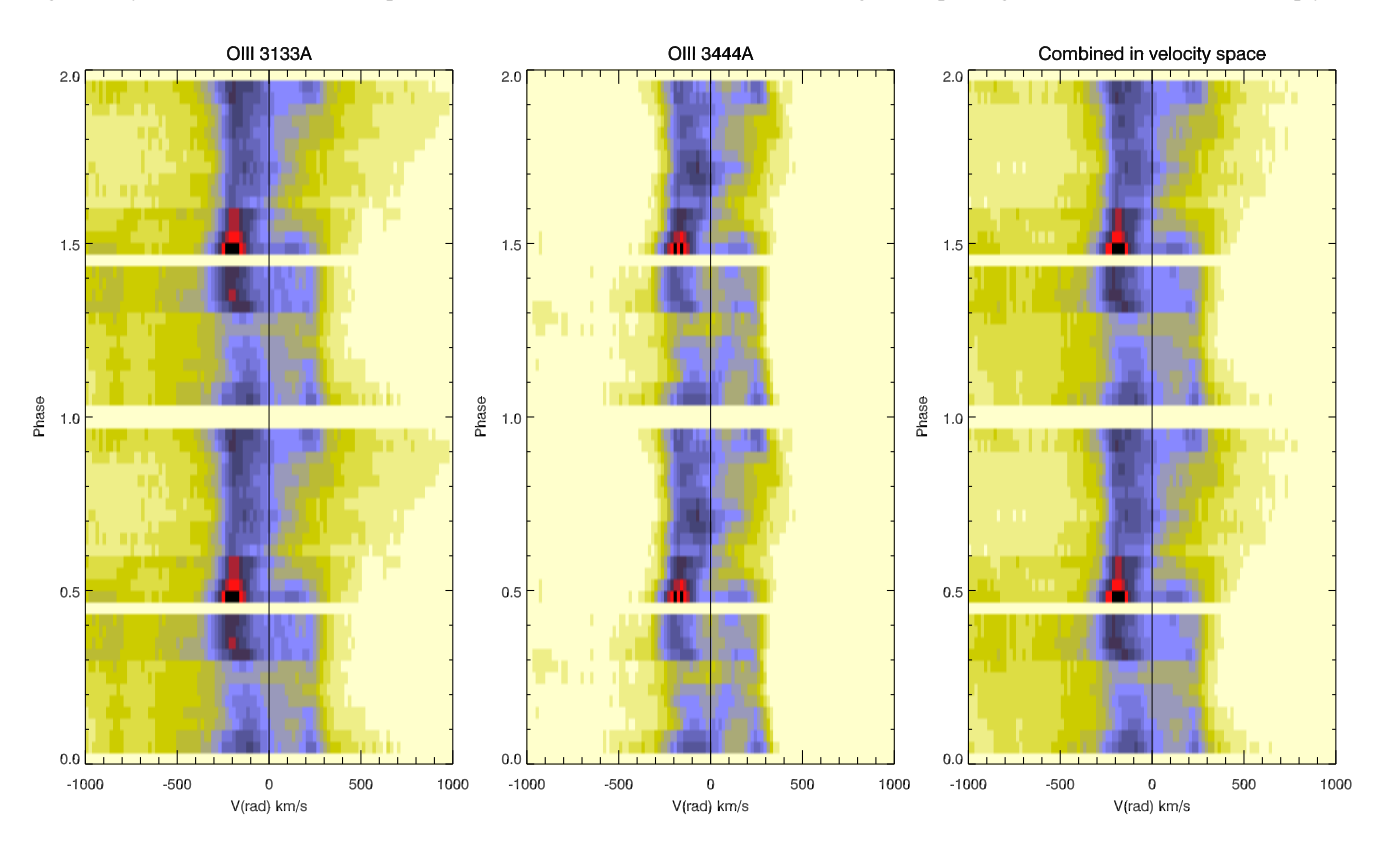


Figure 8. Trailed spectrograms of the O III λ 3133 and λ 3444 emission lines, previously used by H65 for determining the mass ratio of the system. The rightmost spectrogram shows the combined spectrogram of the O III λ 3133 and λ 3444 emission lines, earlier used for lines in velocity space. There is no clear evidence of two spectral components varying in antiphase. Note the inverse flux scale.

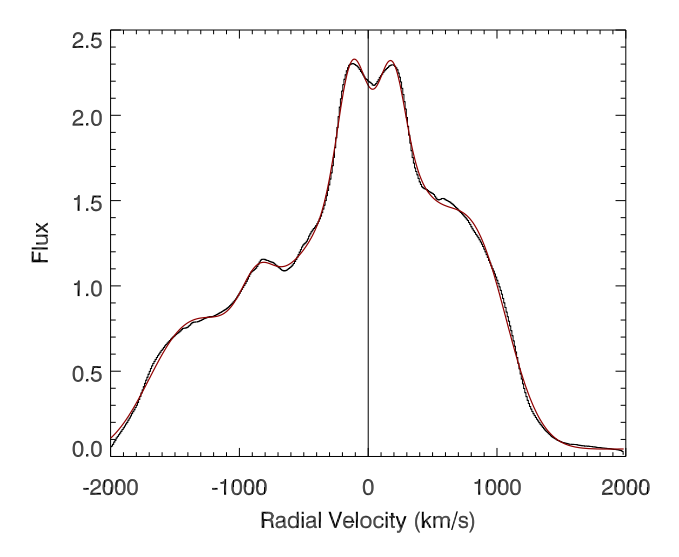


Figure 9. The mean $H\alpha$ line profile together with the best-fitting model (red), consisting of seven Gaussian profiles used to estimate the circumbinary ring velocity.

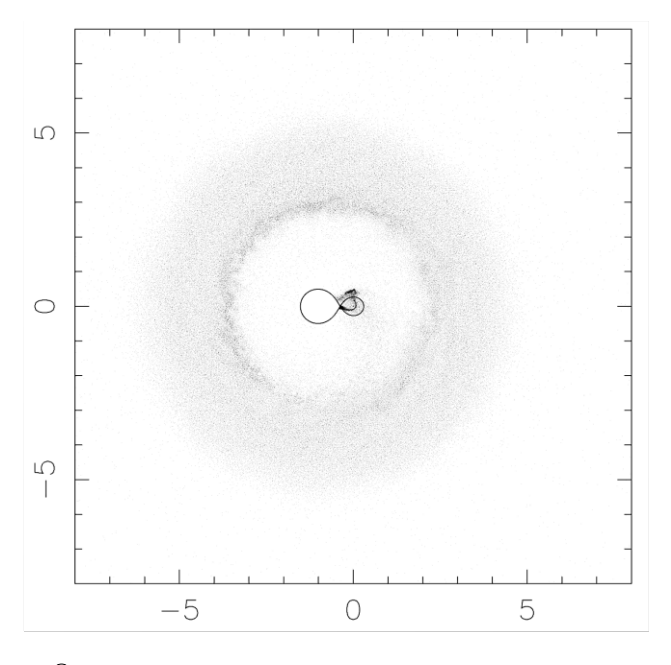
means of expelling matter from the system. In reality, the matter is more likely to be driven out by radiation pressure, resulting from the near-Eddington-limited accretion and/or steady nuclear burning on the WD surface that we believe must be occurring.³

For the simulation, we used $M_1=0.9\,\mathrm{M}_\odot$ and q=3.5. We also experimented with different masses and mass ratios to assess the sensitivity of the simulation results to these parameters. A second simulation was carried out with $M_1=1.25\,\mathrm{M}_\odot$ and q=1, to account for potential uncertainties in the radial velocity curves of H65. In both cases, the simulations produced a circumbinary ring with typical velocities of $\simeq 200\,\mathrm{km\ s^{-1}}(\mathrm{Fig.\ 10})$, and the results did not differ significantly between them.

Our simulations show that, as matter escapes from the WD's Roche lobe, it forms a ring or rings around the binary, with a radius of roughly 2–4 binary separations. The orbital velocity of the matter in such a circumbinary ring is $\approx 200\, km\ s^{-1}$, somewhat larger, but broadly compatible with the double-peak separation we measure in most emission lines.

It is interesting to note that the existence of a circumbinary ring has been proposed previously, based on both theoretical and observational studies. Phillips & Podsiadlowski (2002) simulated mass-loss from luminous X-ray binaries due to the radiation pressure exerted on the donor star, resulting in mass-loss via the outer Lagrangian point and the formation of a circumbinary 'excretion' disc. Blundell, Bowler & Schmidtobreick (2008), on the other hand, observed that the emission line profiles in SS 433 contain two narrow emission components that also do not vary with orbital phase. Their interpretation is similar to ours, i.e. they are likely caused by the presence of a circumbinary disc or ring.

Following the approach taken by Blundell et al. (2008), we can also obtain an independent measure for the total mass of the system as a function of the mass ratio, q. Assuming that the circumbinary ring radius is close to the innermost stable orbit around the binary, we can further estimate the radius of the circumbinary ring to be $R_c \sim F \times a$ (a being the binary separation), where F = 2.2 - 2.3 (Holman & Wiegert 1999). Then, we can use the equation (with



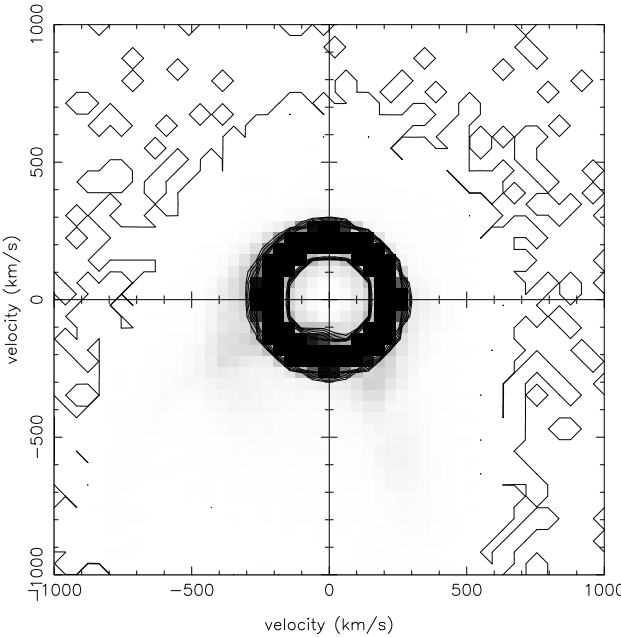


Figure 10. The resulting mass distribution from our simulation, showing the circumbinary ring (top panel; units are in binary separations) and the resulting Doppler tomogram (bottom panel).

$$q = M_{\rm X}/M_2; M_{\rm X} = M_1)$$

$$M_{\rm total} = \frac{V_{\rm c}^2 F V_x P_x}{2\pi G} (1+q) , \qquad (1)$$

where, V_c , V_x , and P_x refer to the circumbinary ring orbital velocity, the primary orbital velocity, and the binary orbital period, to derive an estimate for the total system mass, since we have the measured velocities. To do this, we have adopted a range of values for the inclination (65° to 80°, since the source is partially eclipsing) and $q = M_X/M_2 = 0.1$ to 1.0. If we further adopt F = 2.3 and assume that our maximum $V_x \sin(i) = 250 \,\mathrm{km \ s^{-1}}$ corresponds to the K_1 velocity of the primary, we can compute a grid of possible system masses.

³Detailed simulations of this scenario are beyond the scope of this paper.

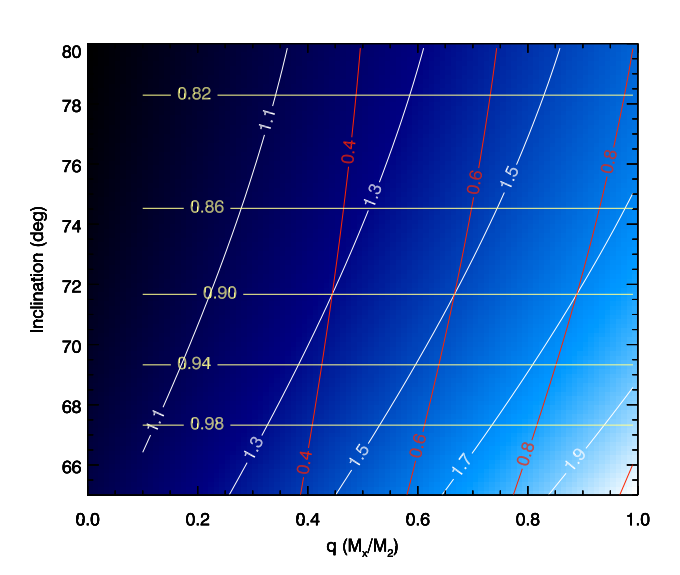


Figure 11. Possible system masses based on the measured circumbinary disc and primary star velocities as a function of q and i. The total masses are shown with the colour map and white contours. The resulting primary masses (M_X) are overplotted with red contours (most vertical), and the donor masses (M_2) with horizontal beige lines.

Combining these with the q values, we can also compute a similar grid for the primary and secondary masses, M_X and M_2 (Fig. 11).

Perhaps the most striking result is that the total mass of the system is constrained to be below 2.1 M_{\odot} for all the q values < 1, with this maximum mass being achieved for q = 1. Furthermore, the primary mass is constrained to be below $\sim 1.0 \, \mathrm{M}_{\odot}$, confirming a WD primary, as is generally assumed. Similarly, the mass of the secondary, M_2 , is constrained to be within $0.8{\text -}1.0\,{\rm M}_{\odot}$ for the $65^{\circ}{\text -}80^{\circ}$ inclination range. Given that the system's intrinsic luminosity is at least 2 dex larger than in any other CV, we have not considered a possibility where the donor star would be less massive (i.e. a normal CV scenario is excluded and the system is assumed to be in the thermally unstable self-accelerating state of mass transfer). Now, given equation (1), we want to consider how strict these derived mass upper limits are. The total mass is quadratically dependent on V_c , but V_c is well constrained by the data, as is P_x . This leaves two possibilities open: perhaps the circumbinary ring is not located at the innermost stable orbit around the binary (i.e. $F \gg 2.3$) or V_x does not reflect the true velocity of the primary. Unfortunately, we cannot answer these questions based on our current data alone.

5.3 Long-term motion of the very broad component

Another puzzling feature in the line profiles is the overall velocity shift of the (very) broad emission wings in strong emission lines, such as H α and He II $\lambda 4686$. Our data show that, while the broad feature moves with orbital phase in contiguous data, its systemic velocity is measured at $-150\,\mathrm{km~s^{-1}}$. However, Gies, Shafter & Wiggs (1998) detected a systemic velocity of $+283\pm5\,\mathrm{km~s^{-1}}$ in their H α study, while an earlier International Ultraviolet Explorer (IUE) FUV spectrum displayed a value of $+700\pm200\,\mathrm{km~s^{-1}}$ (Koch et al. 1986) in He II, C IV, and N v. We then undertook a literature search that revealed a range of systemic velocities for this broad component dating back to 1940 (Elvey & Babcock 1943; H65). We present these in Fig. 12: while no clear long-term periodicity is evident in this $\approx 100\,\mathrm{yr}$ of data, distinct and highly significant changes have occurred throughout this period.

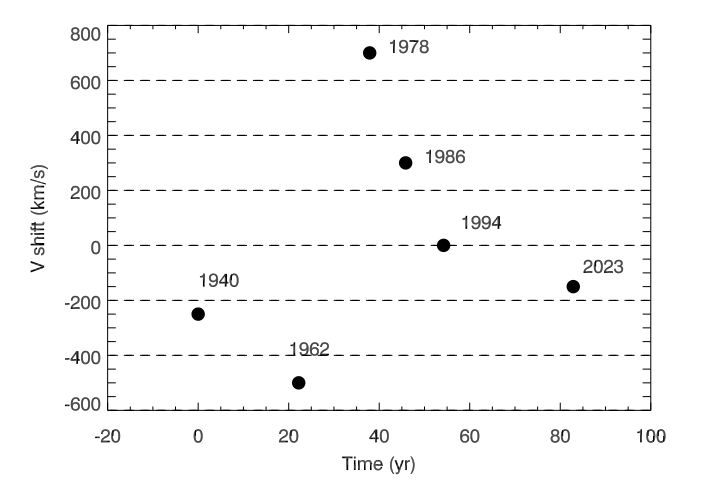


Figure 12. Historical velocity shifts since 1940 (time 0) of the centre of the broad emission line component (from Elvey & Babcock 1943; Herbig et al. 1965; Koch et al. 1986; Robertson, Honeycutt & Pier 1997; Gies et al. 1998, and this work). See also Iijima et al. (2024) for more recent, higher cadence data

To produce such a broad line profile, the highest velocities must originate close to the accreting WD, i.e. within the inner accretion disc, and we observe this feature displaying orbital motion within each cycle. But how, then, do we explain these extraordinary movements on time-scales of years, which produce large, persistently blue- or red-shifted systemic velocities, while the narrow double-peaked feature remains essentially fixed at the binary's true systemic velocity? We propose a possible explanation in which, due to its extremely high luminosity, the inner disc generates a strong, high-velocity wind responsible for the broad emission component. This could account for the overall line profile; however, to produce the large systemic velocity shifts on a time-scale of many years, the disc would need to be tilted and/or warped and to precess over such an interval.

Very recently, Iijima et al. (2024) published the results of 26 yr of optical spectral monitoring of V Sge. They find, as we do, that the source shows episodes of both blue- and red-shifted broad emission components. They also find that, while these states can persist for years, transitions between the blue- and red-shifted states can occur within just 4–5 d, imposing stringent constraints on the underlying physical mechanism. They present the temporal evolution of the broad and narrow line components in their fig. 10.

Upon closer inspection of that figure, we find that the distribution of spectral states is bimodal, with the time the source spends in a blue-or red-shifted state ranging from days to several years. This behaviour appears chaotic, exhibiting two distinct 'modes' with swift transitions between them. Physically, this could be linked to variations in the warping or tilt of the inner accretion disc, occurring on a time-scale of days. The same tilt can then persist for an extended interval (from days to years) before the next 'flipping' event takes place.

We note that Wijers & Pringle (1999) demonstrated through numerical simulations that inner accretion discs become warped and precess due to radiation, *and*, if the radiation is strong enough, the inner disc's tilting behaviour becomes chaotic. According to Smak (2022), the mass transfer rate \dot{M}_2 could be as high as $-2.5 \times 10^{-5} \, \mathrm{M}_{\odot} \, \mathrm{yr}^{-1}$, placing V Sge well above the Eddington limit for a $1 - \mathrm{M}_{\odot}$ WD. It is therefore plausible that chaotic changes in the inner disc inclination are the primary driver of the bimodal velocity shifts observed in the broad component of the emission

lines. We should point out though, that the stability criteria of the inner accretion disc depend strongly on the accretion efficiency and the α parameter for the disc viscosity, as well as the bolometric luminosity, which is not well constrained for V Sge.

5.4 Is V Sge truly an SSS?

While Fig. 7 demonstrates the presence of very soft X-rays during the ROSAT May 1994 observation of V Sge during a faint state, we do not have a precise knowledge of its actual luminosity. This is partly because the ROSAT HRI (High Resolution Imager) was only intended to be used as an X-ray imager, and so detailed spectral modelling is not possible. However, this was also noted by Greiner & Teeseling (1998), whose fig. 2 (top) gives the L_X-T contours for fitting their strongest 'intermediate' state 'soft X-ray' spectrum, which was obtained with the ROSAT PSPC (Position Sensitive Proportional Counter) detector. At first sight, this appears to suggest only a low $L_{\rm X}$ value of $\sim 10^{32}\,{\rm erg\,s^{-1}}$ (we have corrected for the now known distance of 3.03 kpc, whereas Greiner & Teeseling used 1 kpc), far below that expected for an SSS component. However, when including the effects of an intervening absorbing column (we used HEASARC's $N_{\rm H}$ tool to calculate $N_{\rm H} = 1.56 \times 10^{21} \, {\rm cm}^{-2}$), then their spectra require much higher $L_{\rm X}$ values, exceeding $10^{36}\,{\rm erg\,s^{-1}}$, in order for the SSS component (likely $T < 5 \times 10^5$ K) to penetrate this material.

5.5 Classifying V Sge: where does it fit?

Finally, we discuss the nature of V Sge and the implications of our new spectral data set. For several decades now, two different models have been proposed to describe the observed behaviour of the system. The original model of H65 assumes a hot binary system, in which both components are hot stars ($T_{\rm WD}=44\,000\,{\rm K}$ and $T_{\rm donor}=22\,000\,{\rm K}$). This was also advocated by Lockley et al. (1999) and Wood & Lockley (2000), who claim that the emission-line profiles can be reproduced by a model involving colliding winds from such stars. This was also strongly preferred by Smak (2022).

The second proposed model for V Sge suggests that it is a high-inclination Galactic SSS (Greiner & Teeseling 1998), i.e. a WD accreting matter from a more massive companion star via (unstable) thermal-time-scale Roche lobe overflow, as introduced in Section 1.1 and modelled by Hachisu & Kato (2003). The resulting accretion rate is so high that it can sustain 'steady' nuclear burning on the WD surface (van den Heuvel et al. 1992). In such cases, the optical emission would be dominated by the accretion disc rather than by either of the two stars.

To compare the merits of both models, we have compiled a list of the observed properties of V Sge in Table 2, and assessed how well they align with each model. While the hot binary model can explain about half of the listed properties, it fails to account for many crucial observed features. In particular, it does *not* explain the system's variability on either short-term (light curve shape changes over days) or long-term (low versus high state) time-scales. Additionally, the mechanism by which such a hot binary would generate extremely strong H α emission remains unclear. H α is the second strongest emission line in the system after He II λ 4686. Finally, the presence of stationary, double-peaked narrow emission lines would still necessitate the formation of a disc or ring around the binary, the origin of which remains unexplained within the hot binary model.

Table 2. Comparison of different properties of V Sge and suggested models.

Property	Supersoft X-ray source	Hot binary
Supersoft X-rays	✓	
High and low states	✓	
Strong Balmer lines	✓	
Highly ionized O, N, and C	✓	/
Complex line profiles	✓	/
Non-variable line cores	✓?	
Rapidly changing eclipse depths	✓	
Overall mean optical light curve	✓	✓
shape		
Emission lines with	✓	✓?
$FWZI > 3200 \mathrm{km \ s^{-1}}$		
Changing orbital period	✓	✓?
Broad component velocity shifts	√ ?	

6 CONCLUSIONS

Our X-Shooter spectroscopic observing campaign of V Sge has reaffirmed the complexity of this system, highlighting that fully understanding its nature remains a significant challenge. Based on the presence of narrow emission-line components during the high state, we argue that V Sge likely hosts a circumbinary ring or disc. Historical data, together with recent spectroscopic monitoring (Iijima et al. 2024), suggest that the long-term variations in the mean velocity of the very broad component are probably driven by the chaotic behaviour of the inner accretion disc under intense irradiation. This interpretation aligns well with simulations by Wijers & Pringle (1999).

We also raise doubts about the canonical radial velocity curves presented by H65, and consequently question the mass ratio and component masses derived from them. Our own dynamical analysis indicates that V Sge is likely a low-mass system, with a total mass less than $2.1\,M_{\odot}$. To test this hypothesis, high-resolution spectroscopic observations, particularly during the system's faint state, are essential. Finally, from the observational properties summarized in Table 2, we conclude that V Sge is driven by an SSS component, which appears to be the most luminous of its kind currently known in the Galaxy.

ACKNOWLEDGEMENTS

First, we thank the anonymous referee for a very constructive report with suggestions that we feel have greatly helped with the presentation of a large, complex data set. We would also like to thank Graham Wynn for access to his HYDISC magnetic accretion simulation code. PAC is grateful to Marina Orio for useful discussions on the SSS component of V Sge, and to Katherine Blundell regarding the circumbinary ring interpretation. PAC acknowledges the Leverhulme Trust for an Emeritus Fellowship, and UKRI for their ESO support. PR-G acknowledges support by the Spanish Agencia Estatal de Investigación del Ministerio de Ciencia e Innovación (MCIN/AEI) and the European Regional Development Fund (ERDF) under grant PID2021–124879NB–100.

DATA AVAILABILITY

The X-shooter spectra are publicly available from the ESO data archive and the fully zoomable plot of the mean spectrum from the included link.

REFERENCES

Abril J., Schmidtobreick L., Ederoclite A., López-Sanjuan C., 2020, MNRAS,

Blundell K. M., Bowler M. G., Schmidtobreick L., 2008, ApJ, 678, L47

Diaz M. P., 1999, PASP, 111, 76

Elvey C. T., Babcock H. W., 1943, ApJ, 97, 412

Eracleous M., Halpern J., Patterson J., 1991, ApJ, 382, 290

Freudling W., Romaniello M., Bramich D. M., Ballester P., Forchi V., García-Dabló C. E., Moehler S., Neeser M. J., 2013, A&A, 559, A96

Gaia Collaboration, 2023, A&A, 674, A1

Gies D. R., Shafter A. W., Wiggs M. S., 1998, AJ, 115, 2566

Greiner J., Teeseling A., 1998, A&A, 339, L21

Hachisu I., Kato M., 2003, ApJ, 598, 527

Herbig G. H., Preston G. W., Smak J., Paczynski B., 1965, ApJ, 141, 617 (H65)

Hoard D. W., Wallerstein G., Willson L. A., 1996, PASP, 108, 81

Holman M. J., Wiegert P. A., 1999, AJ, 117, 621

Iijima T., Naito H., Narusawa S.-y., 2024, PASJ, 76, 1002

Kahabka P., 1997, in Makino F., Mitsuda K., eds, X-Ray Imaging and Spectroscopy of Cosmic Hot Plasmas. Universal Academy Press, Tokyo, p. 435

Kato T., 2004, PASJ, 56, S133

King A. R., 1993, MNRAS, 261, 144

Koch R. H., Corcoran M. F., Holenstein B. D., McCluskey G. E. J., 1986, ApJ, 306, 618

Lockley J. J., Wood J. H., Eyres S. P. S., Naylor T., Shugarov S., 1999, MNRAS, 310, 963

Marsh T. R., Horne K., 1988, MNRAS, 235, 269

Meyer-Hofmeister E., Schandl S., Meyer F., 1997, A&A, 321, 245

Patterson J. et al., 1998, PASP, 110, 380

Phillips S. N., Podsiadlowski P., 2002, MNRAS, 337, 431

Robertson J. W., Honeycutt R. K., Pier J. R., 1997, AJ, 113, 787

Rodríguez-Gil P. et al., 2007, MNRAS, 377, 1747

Schneider D. P., Young P., 1980, ApJ, 238, 946

Shafter A. W., 1983, ApJ, 267, 222

Shafter A. W., 1983, ApJ, 267, 22 Simon V., 2003, A&A, 406, 613

Šimon V., Mattei J. A., 1999, A&AS, 139, 75

Smak J., 2022, Acta Astron., 72, 21

Smak J. I., Belczynski K., Zola S., 2001, Acta Astron., 51, 117

Southwell K. A., Livio M., Charles P. A., O'Donoghue D., Sutherland W. J., 1996, ApJ, 470, 1065

Spruit H. C., 1998, preprint (arXiv:astro-ph/9806141)

Steiner J. E., Diaz M. P., 1998, PASP, 110, 276

Storn R., Price K., 1997, J. Glob. Opt., 11, 341

Thorstensen J. R., Ringwald F. A., Wade R. A., Schmidt G. D., Norsworthy J. E., 1991, AJ, 102, 272

van den Heuvel E. P. J., Bhattacharya D., Nomoto K., Rappaport S. A., 1992, A&A, 262, 97

Vernet J. et al., 2011, A&A, 536, A105

Wijers R. A. M. J., Pringle J. E., 1999, MNRAS, 308, 207

Wood J. H., Lockley J. J., 2000, MNRAS, 313, 789

Wynn G. A., King A. R., 1995, MNRAS, 275, 9

Zang L., Qian S., Zhu L., Liu L., 2022, MNRAS, 511, 553

Zemko P., Orio M., Mukai K., Shugarov S., 2014, MNRAS, 445, 869

APPENDIX A: TRAILED SPECTRA PLOTS

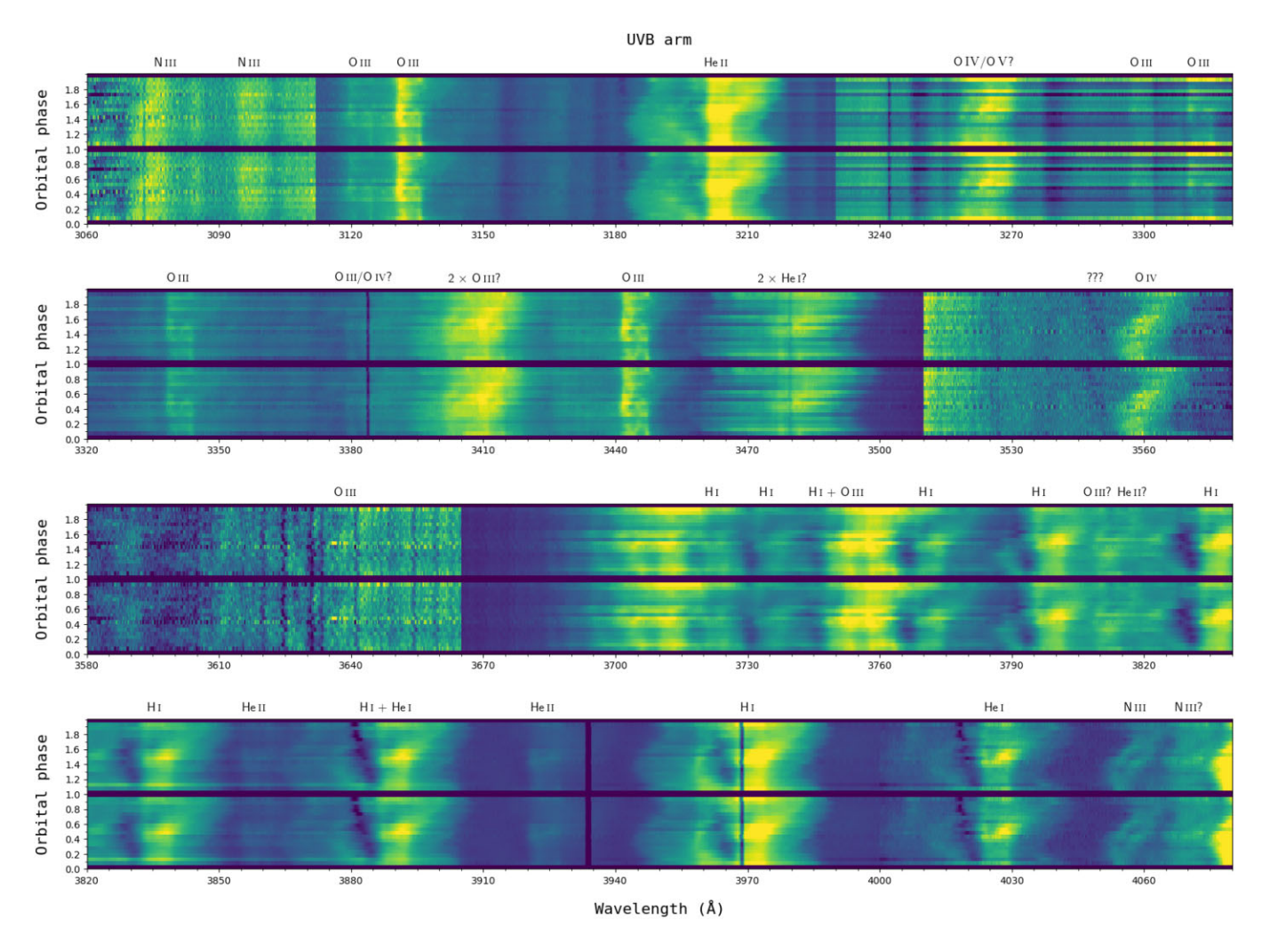


Figure A1. X-Shooter UVB arm trailed spectra diagrams using all the data averaged into 20 orbital phase bins. The full cycle has been repeated once for clarity.

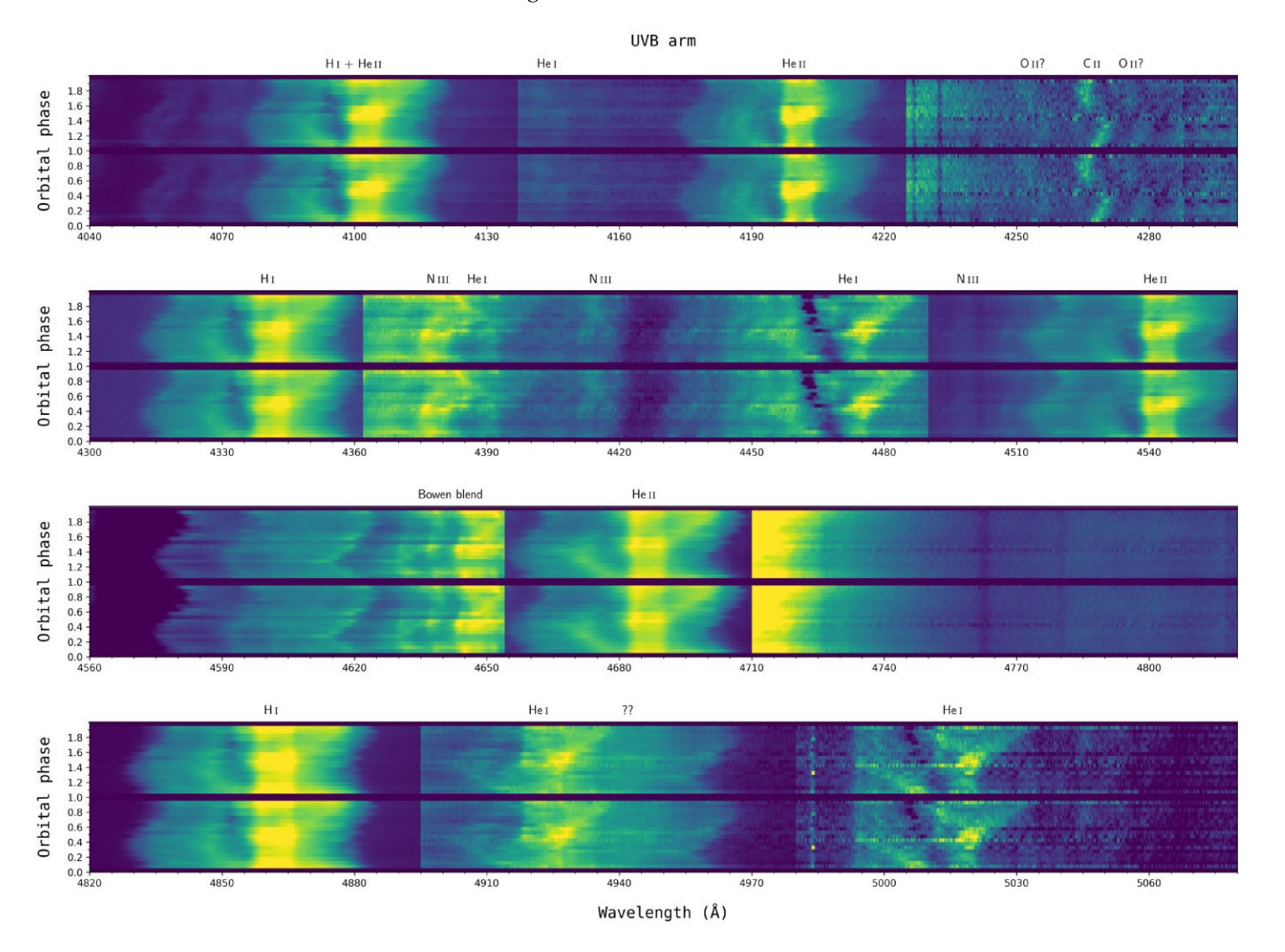


Figure A1. - continued

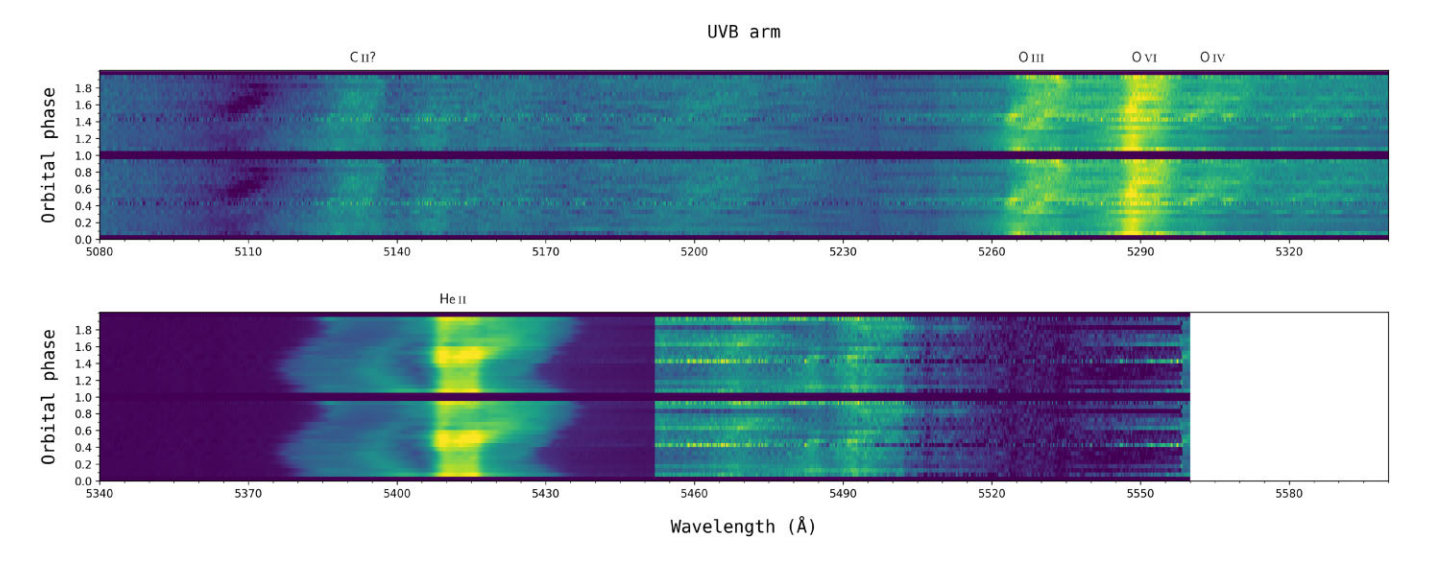


Figure A1. - continued

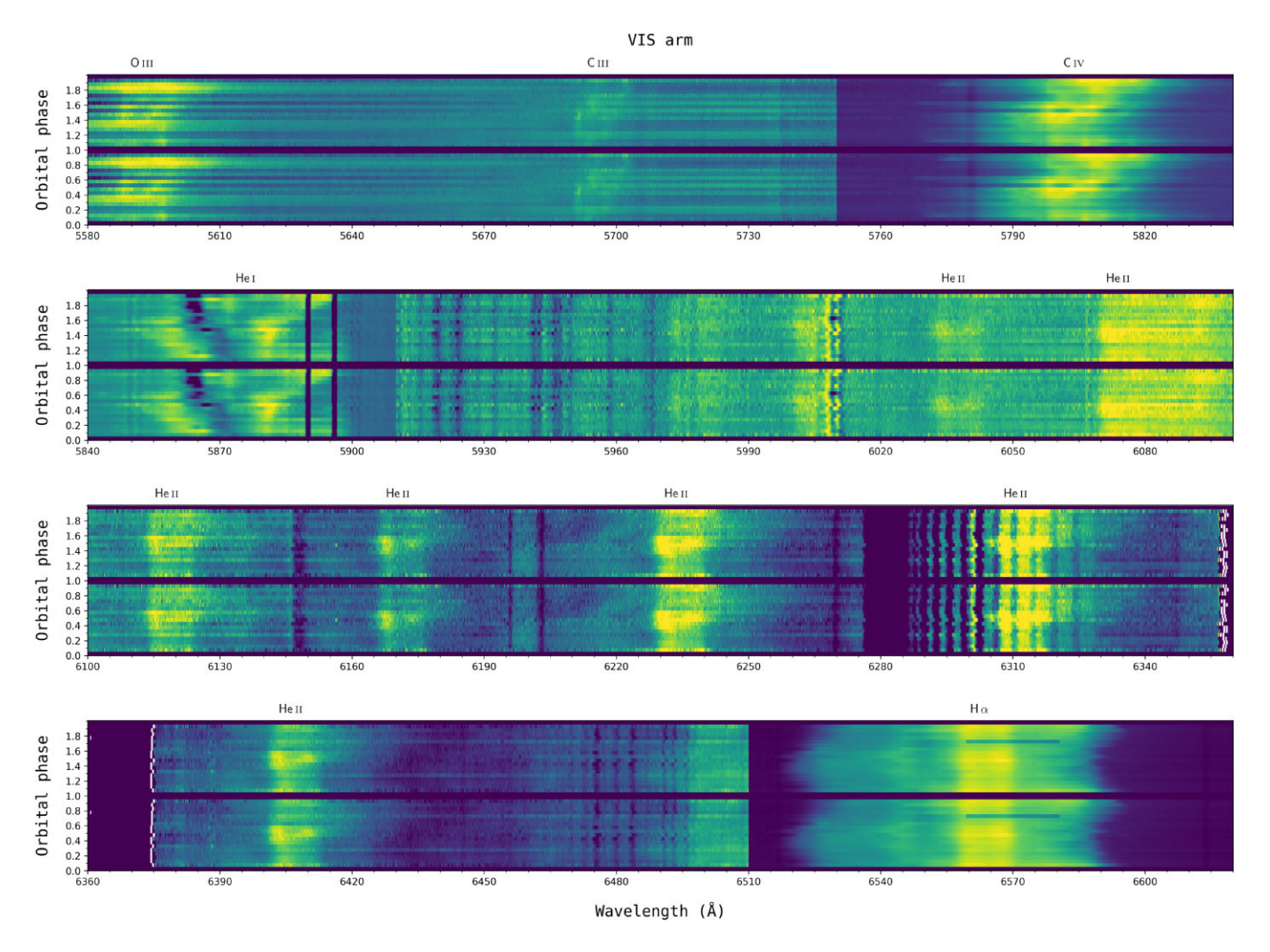


Figure A2. X-Shooter VIS arm trailed spectra diagrams using all the data averaged into 20 orbital phase bins. The full cycle has been repeated once for clarity.

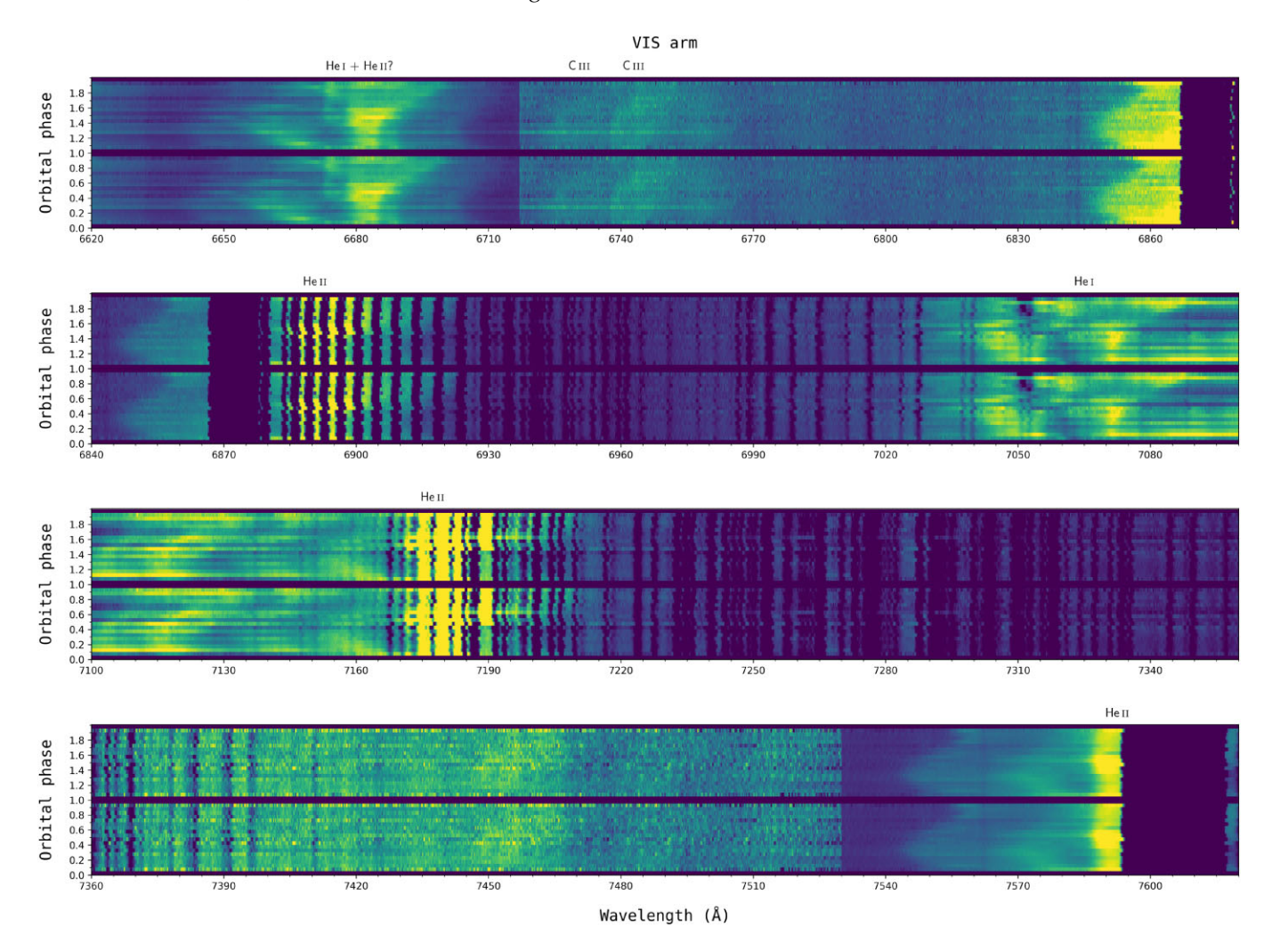


Figure A2. - continued

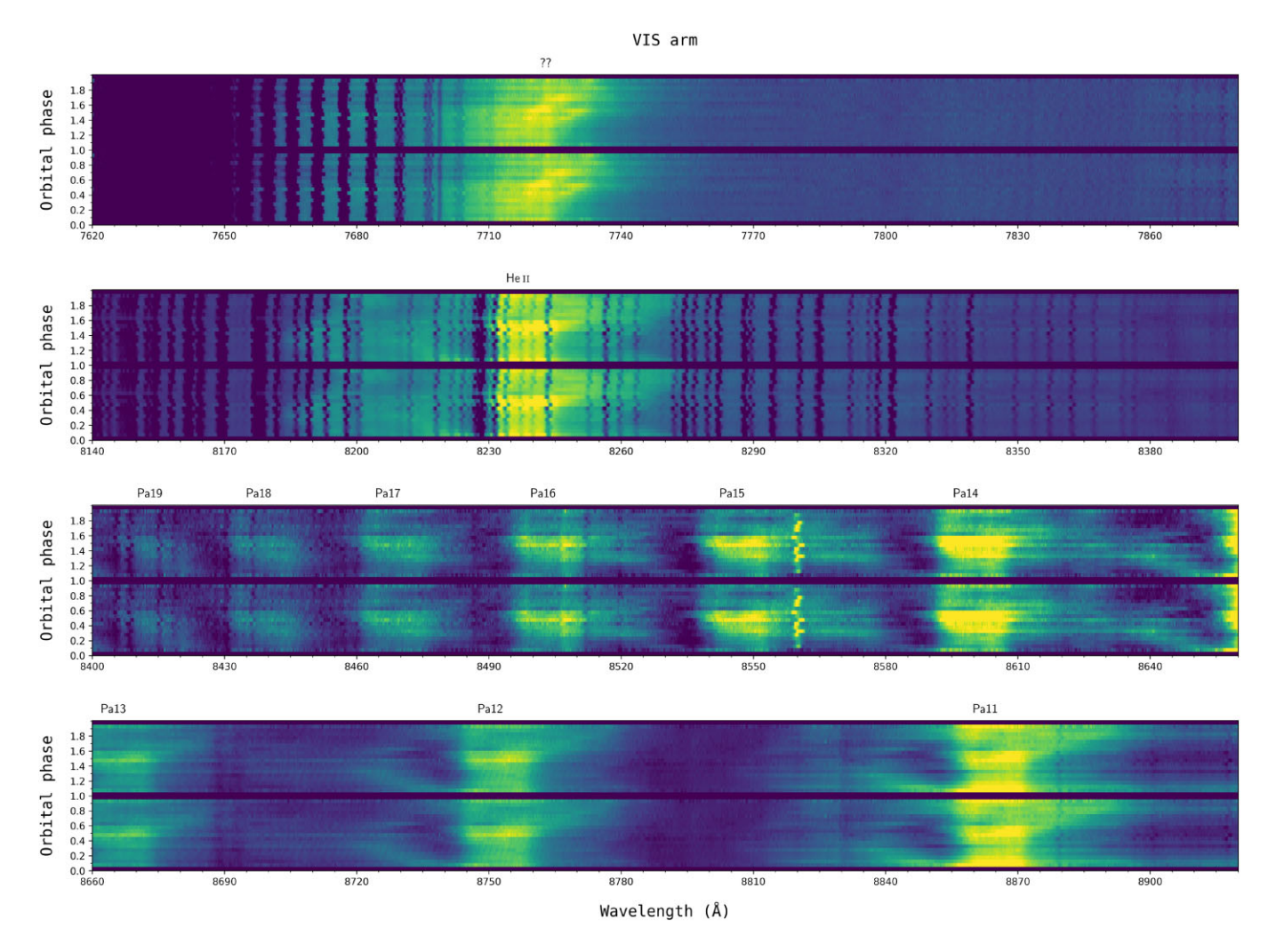


Figure A2. - continued

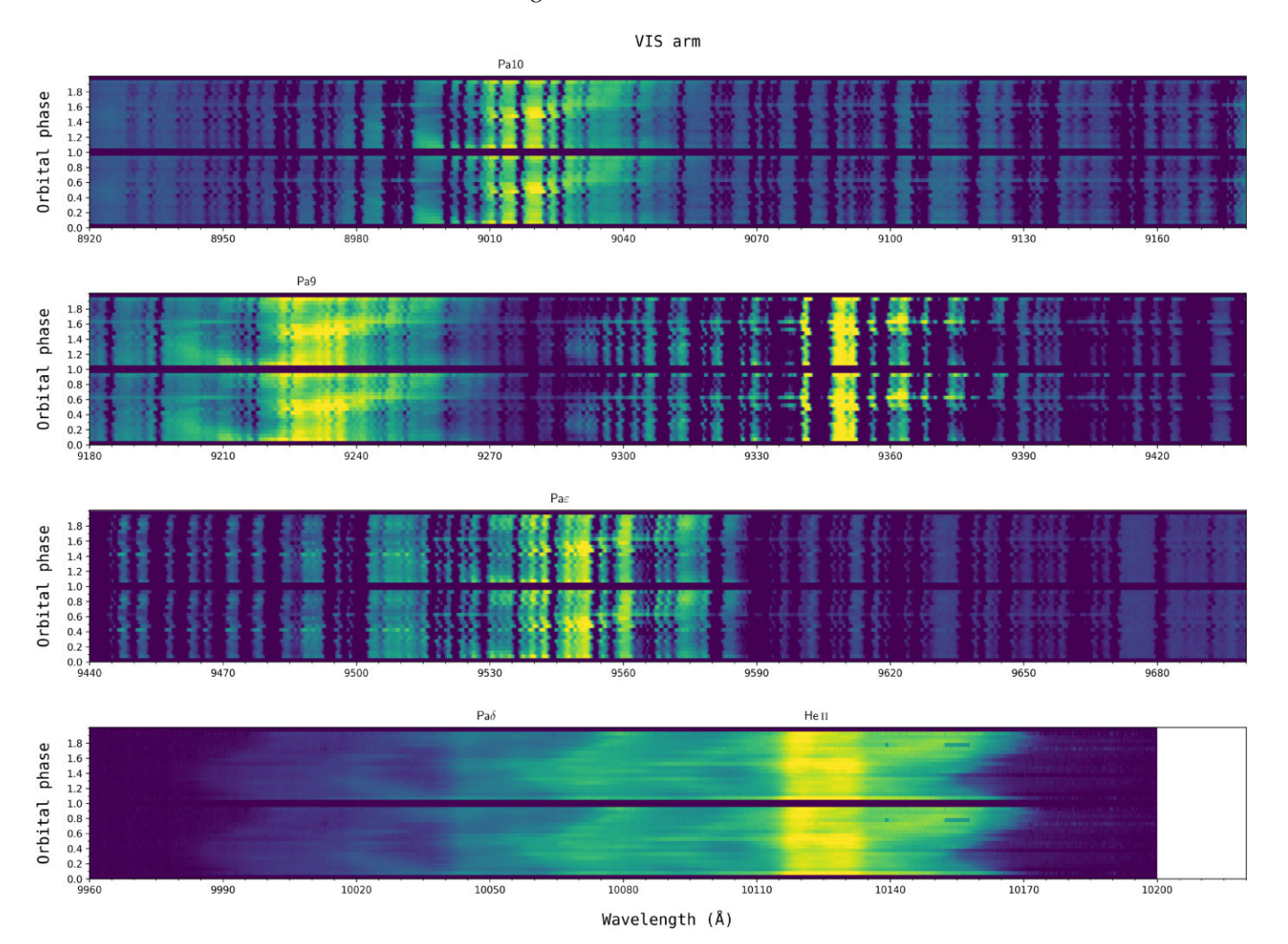


Figure A2. - continued

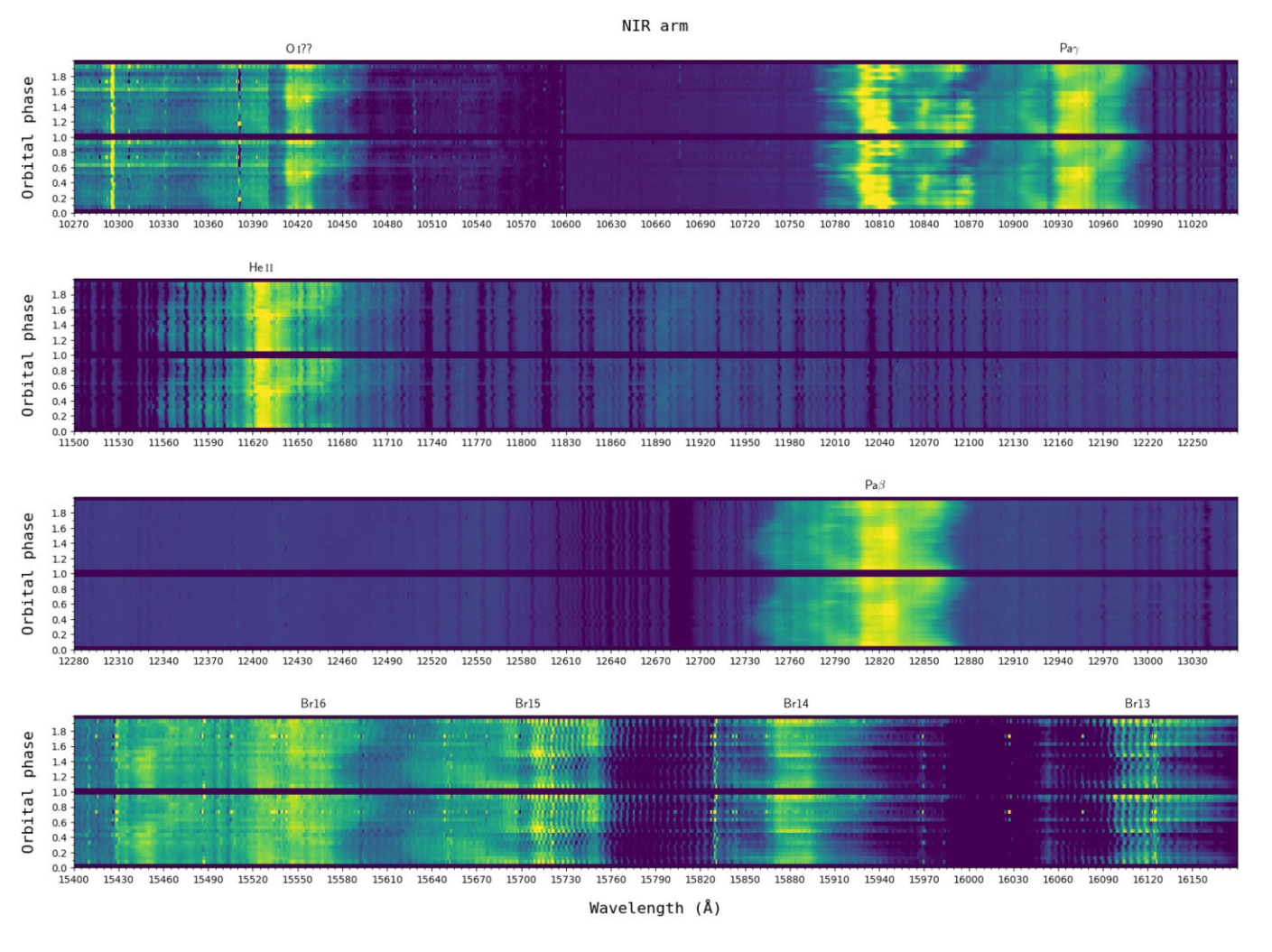


Figure A3. X-Shooter NIR arm trailed spectra diagrams using all the data averaged into 20 orbital phase bins. The full cycle has been repeated once for clarity.

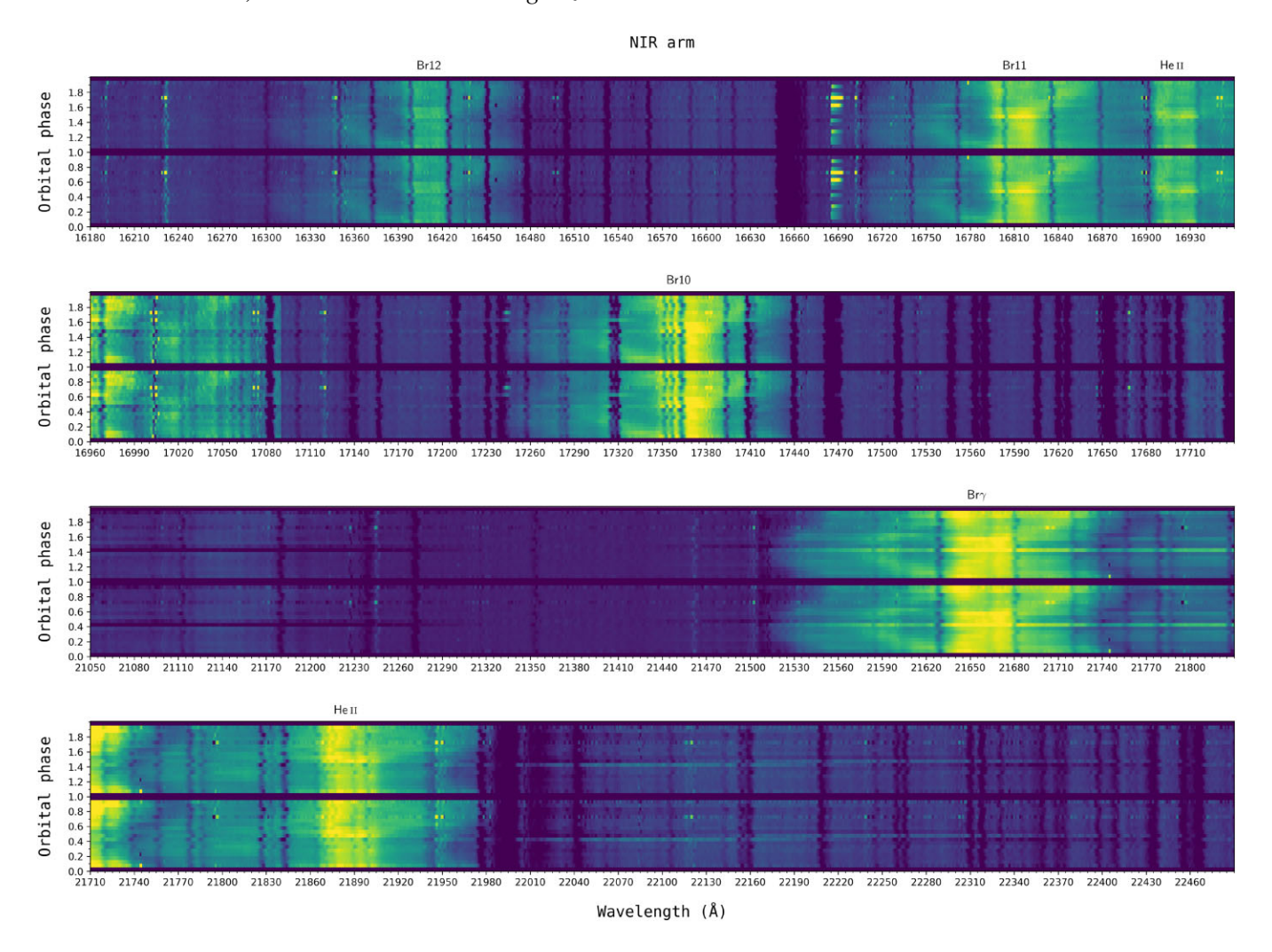


Figure A3. – continued

APPENDIX B: THE KINEMATIC ANALYSIS OF SPECTRAL LINE WINGS

Since the emission-line profiles in V Sge are very complex and consist of multiple components, it is not trivial to extract the orbital velocities of the stellar components. In particular, we do not detect *any* spectroscopic signal that could be associated with the donor star. However, the very broad wings of the emission lines do appear to follow approximately the predicted movement of the primary (accreting) component, that is eclipsed at phase 0. In order to extract/measure this movement (i.e. determine the K velocity of the primary), we initially utilized the double-Gaussian approach (Schneider & Young 1980; Shafter 1983) with a Gaussian width of 250 km s⁻¹, as described in Section 3.1.2.

As the results from the double-Gaussian analysis were not entirely conclusive (Fig. B1), we developed another method that we call

'wing-folding'. In this technique, we apply an exclusion window (of variable extent) to the central part of the emission line profile and compare the relative flux of the line remaining in the blue and red wings for different values of the line central velocity. The best radial velocity for each line profile is then determined by looking for a line-wing flux ratio V/R = 1. Applying this method for different widths of the central exclusion region produces a similar diagnostic diagram to the double-Gaussian method, but is independent of any functional form for the line wings. We show here the diagnostic diagrams using both methods (Fig. B1). We conclude from these that the observed K velocity is very likely in the $200-250 \,\mathrm{km \ s^{-1}}$ range. Given that partially eclipses are seen in the light curve, the inclination must be above $\approx 65^{\circ}$, i.e. the real K has an upper limit of 220–275 km s⁻¹. We also find that the γ velocity of the central accretion disc, where we presume the high-velocity wing emission originates, is approximately $-150 \,\mathrm{km \ s^{-1}}$.

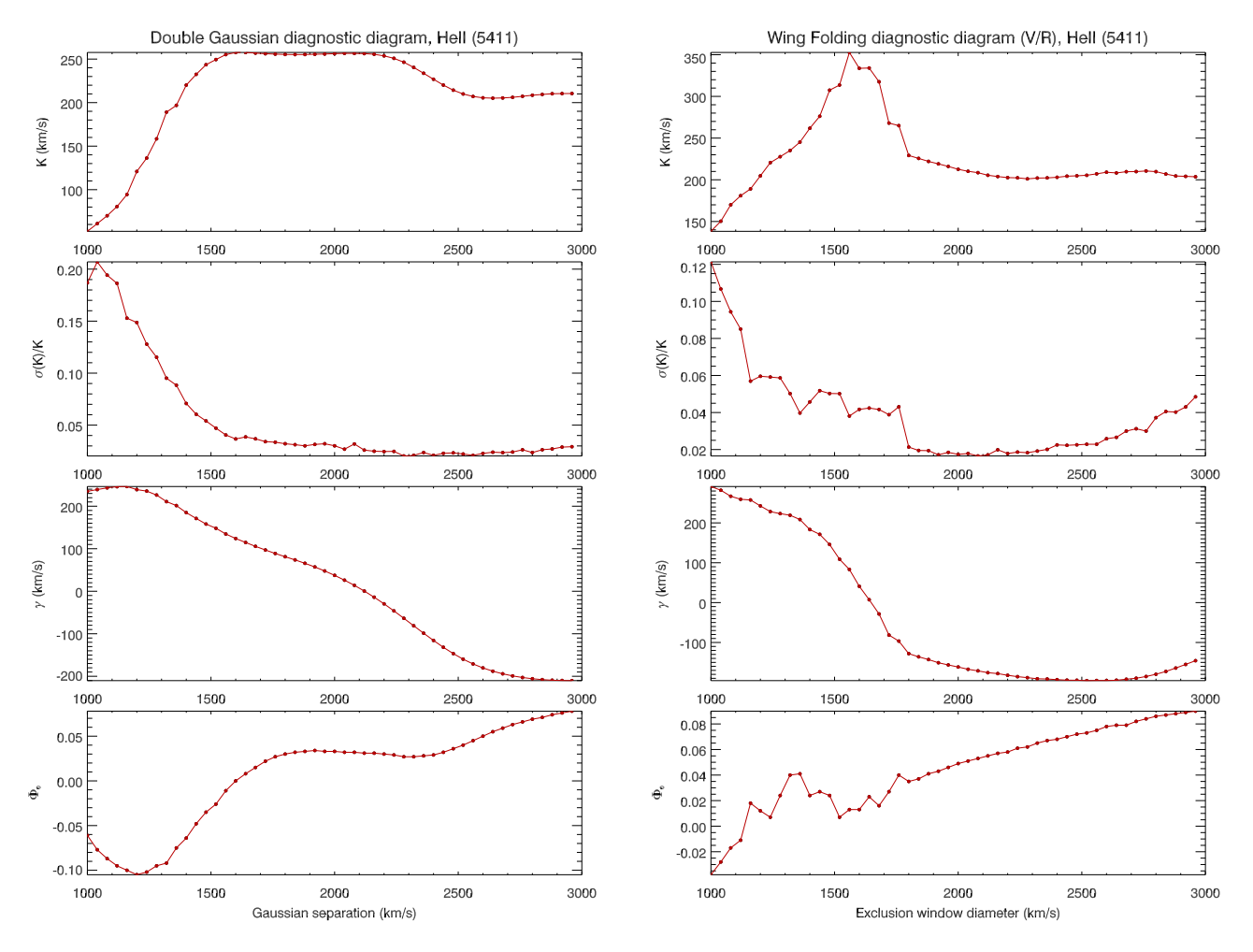


Figure B1. Comparison of diagnostic diagrams obtained using the double-Gaussian method (left) and the newly developed 'wing-folding' technique (right).

This paper has been typeset from a TEX/LATEX file prepared by the author.